

# Comparison of 2D and 3D models of flow structure in semidetached binaries

D.V.Bisikalo<sup>1</sup>, A.A.Boyarchuk<sup>1</sup>,  
V.M.Chechetkin<sup>2</sup>, O.A.Kuznetsov<sup>2</sup>, D.Molteni<sup>3</sup>

<sup>1</sup> Institute of Astronomy of Russian  
Academy of Sciences, Moscow

<sup>2</sup> Keldysh Institute of Applied Mathematics, Moscow

<sup>3</sup> Dipartimento di Scienze Fisiche ed Astronomiche,  
Università di Palermo

**Abstract**—We present the results of systematic comparison of 2D and 3D numerical models of mass transfer in semidetached binaries. It is shown that only for case of  $\gamma \sim 1$  (near-isothermal case) the obtained 2D and 3D solutions are qualitatively similar. For higher value of  $\gamma$  the 3D flow structure is drastically changed and for  $\gamma = 1.2$  the accretion disk is not formed in the system. Numerical results show that for case of  $\gamma = 1.2$  the 2D and 3D solutions are different.

We discuss the spiral-shaped shock waves obtained in numerical models. It is shown that these shocks are not intrinsic spirals and are caused by collisions of the gaseous flows in the system.

## INTRODUCTION

The semidetached binaries are the interacting stars, where one component fills its Roche lobe and mass transfer between components of the system occurs through the vicinity of inner Lagrangian point  $L_1$ . The semidetached binaries – cataclysmic variables, low-mass X-ray binaries, supersoft X-ray sources, etc. – show a lot of bright evidences of a complex flow structure that should be interpreted. Since the pioneer work by Prendergast [1] the gasdynamical treatment of the flow patterns in semidetached binaries have been made by many workers. The numerical simulations were conducted both in 2D (see, e.g., [2–8]) and in 3D ([9–20]) models. For a long time the 3D numerical simulation was limited by computer power therefore the 2D models were the preferred ones for the analysis of the flow structure. A lot of interesting results were obtained using the two-dimensional approach and a set of bright ideas were based on this numerical simulations. The known restrictions of the 2D approach cause the question of the validity of used models and of reliability of obtained

results. The question of the 2D approach applicability became especially important since 1994 when Fridman & Khoruzhii [21] have analytically shown that in the accretion disk the 2D approach is valid only for two specific cases (for isothermal disk under the action of external gravitational field, and for self-gravitating disk with heats ratio  $\gamma = 2$ ), while for all other cases the only 3D models are valid.

It is evident that the direct way to estimate the applicability of 2D models is the comparison of 2D and 3D results. Unfortunately, the comparison between results obtained earlier in 2D and 3D models by previous authors is rather difficult because they have used different numerical technics and have considered different binary parameters. To be confirmed in the results of a comparison it is necessary to perform a set of 2D and 3D simulation using the same numerical technique for the same binary system and for the same boundary conditions. The only one attempt to make such comparison is due to Sawada and Matsuda [12], but their 3D calculations were rather crude due to bad spatial resolution and small time of calculations (they have stopped the run at the time less than a half of orbital period, i.e. when the steady-state regime was not established). Therefore, while the authors have declared the qualitative similarity of 2D and 3D results this conclusion was not well argued.

In the present work, for the first time, we have made the systematic comparison of the 2D and 3D models. We perform two- and three-dimensional hydrodynamic simulation of the flow of inviscid adiabatic gas in a non-magnetic semidetached binary. The description of the used models are presented in Section 2. The 3D runs is very time-consuming, nevertheless in 3D model we use the rather fine grid (only 2 times coarser than in 2D model) and conduct the runs up to the steady-state flow regime (up to 10 orbital periods) which allows us to make a reliable comparison with 2D results. In Section 3 it is shown that the qualitative similarity of 2D and 3D results exists only for the case of the  $\gamma \sim 1$ , while for higher  $\gamma$  the solutions are different. In Section 4 we discuss the changes of the flow structure caused by different values of  $\gamma$ .

One of the most interesting numerical results obtained in previous works is the presence of two-armed spiral shocks in accretion disk. In a set of numerical and analytical works (see, e.g., [2–5,12]) these shocks have been considered as intrinsic spiral shocks caused by the tidal disturbances of accretion disk. The set of 2D and 3D runs, conducted in the present work, shows the existence of spiral-shape shocks in the semidetached binaries, but as it follows from the analysis of results these shocks are caused by collision of gas fluxes in the system. In Section 5 we discuss the proves of the "flow crossing" nature of obtained spiral-shaped shocks. Our conclusions follow in Section 6.

## 1 THE MODEL DESCRIPTION

To compare results of this work with previous ones we study the non-magnetic binary system with the same parameters as in [2]. We consider a semi-detached binary with components mass ratio of unity. The mass-losing star fills up its critical Roche lobe that causes the mass transfer between components of the system.

To describe the gas flow in the binary we use the standard Euler equations in the reference frame corotating with the binary system. The 3D simulations are made in Cartesian coordinates  $(x, y, z)$  and the equations have the form:

$$\begin{aligned}
\frac{\partial \rho}{\partial t} + \frac{\partial \rho u}{\partial x} + \frac{\partial \rho v}{\partial y} + \frac{\partial \rho w}{\partial z} &= 0 \\
\frac{\partial \rho u}{\partial t} + \frac{\partial}{\partial x}(\rho u^2 + P) + \frac{\partial \rho uv}{\partial y} + \frac{\partial \rho uw}{\partial z} &= -\rho \frac{\partial \Phi}{\partial x} + 2\Omega v \rho \\
\frac{\partial \rho v}{\partial t} + \frac{\partial \rho uv}{\partial x} + \frac{\partial}{\partial y}(\rho v^2 + P) + \frac{\partial \rho vw}{\partial z} &= -\rho \frac{\partial \Phi}{\partial y} - 2\Omega u \rho \\
\frac{\partial \rho w}{\partial t} + \frac{\partial \rho uw}{\partial x} + \frac{\partial \rho vw}{\partial y} + \frac{\partial}{\partial z}(\rho w^2 + P) &= -\rho \frac{\partial \Phi}{\partial z} \\
\frac{\partial \rho E}{\partial t} + \frac{\partial \rho uh}{\partial x} + \frac{\partial \rho vh}{\partial y} + \frac{\partial \rho wh}{\partial z} &= -\rho u \frac{\partial \Phi}{\partial x} - \rho v \frac{\partial \Phi}{\partial y} - \rho w \frac{\partial \Phi}{\partial z} .
\end{aligned}$$

Here  $\rho$  – density;  $\mathbf{v}(x, y, z) = (u, v, w)$  – velocity vector;  $P$  – pressure;  $E$  – specific full energy  $E = \varepsilon + \mathbf{v}^2/2$ ;  $\varepsilon$  – internal specific energy;  $h$  – specific full enthalpy  $h = \varepsilon + P/\rho + \mathbf{v}^2/2$ ;  $\Phi$  – Roche potential

$$\Phi(\mathbf{r}) = -\frac{GM_1}{|\mathbf{r} - \mathbf{r}_1|} - \frac{GM_2}{|\mathbf{r} - \mathbf{r}_2|} - \frac{1}{2}\Omega^2 (\mathbf{r} - \mathbf{r}_c)^2 ,$$

where  $\mathbf{r}_1, \mathbf{r}_2$  – the centers of components of the system; and  $\mathbf{r}_c$  – the center of mass of the system;  $M_1, M_2$  – masses of components;  $\Omega = 2\pi/P_{\text{orb}}$  – angular velocity of the system.

The 2D simulations are made in cylindrical coordinates  $(r, \phi)$  and the equations have the form:

$$\begin{aligned}
\frac{\partial \rho}{\partial t} + \frac{1}{r} \frac{\partial r \rho u}{\partial r} + \frac{1}{r} \frac{\partial \rho v}{\partial \varphi} &= 0 \\
\frac{\partial \rho u}{\partial t} + \frac{1}{r} \frac{\partial}{\partial r}(r \rho u^2 + r P) + \frac{1}{r} \frac{\partial \rho uv}{\partial \varphi} &= \frac{P}{r} - \rho \frac{\partial \Phi}{\partial r} + \rho \frac{v^2}{r} + 2\Omega v \rho \\
\frac{\partial \rho v}{\partial t} + \frac{1}{r} \frac{\partial r \rho uv}{\partial r} + \frac{1}{r} \frac{\partial}{\partial \varphi}(\rho v^2 + P) &= -\frac{\rho}{r} \frac{\partial \Phi}{\partial \varphi} - \rho \frac{uv}{r} - 2\Omega u \rho \\
\frac{\partial \rho E}{\partial t} + \frac{1}{r} \frac{\partial r \rho uh}{\partial r} + \frac{1}{r} \frac{\partial \rho vh}{\partial \varphi} &= -\rho u \frac{\partial \Phi}{\partial r} - \rho \frac{v}{r} \frac{\partial \Phi}{\partial \varphi} ,
\end{aligned}$$

where  $\mathbf{v}(r, \varphi) = (u, v)$  – velocity vector.

Both for 2D and 3D cases we used the ideal gas equation of state  $P = (\gamma - 1)\rho\varepsilon$  where  $\gamma$  is the ratio of specific heats. Following to procedure suggested by [2] the 2D and 3D equations are adimensionalized using the separation  $A$  of the two stars as the length scale, the reciprocal of the orbital angular velocity ( $\Omega^{-1}$ ) as the time-scale and the density on the surface of mass-losing star as the density scale. The used velocity scale is  $A\Omega$ .

To specify the physical boundary conditions on the Roche lobe of the mass-losing star we have to settle the density ( $\rho_0$ ), sound velocity ( $c_0$ ), and gas velocity vector  $\mathbf{v}_0$ . It should be noted however that: i) the boundary value of density on the surface of mass-losing star has no influence on the solution, due to scaling of the system of equations with respect to  $\rho$

(with simultaneous scaling of  $P$ ), and ii) in adimensioned approach the used value of sound velocity can correspond to arbitrary value of the temperature in dependence of adopted physical values of  $M_1$ ,  $M_2$  and  $A$ . Therefore to compare results with previous ones we have adopted the same adimensioned gas parameters at the surface of mass-losing star as in the work by [2]:

- the value of density  $\rho_0$  is equal to 1;
- sound speed  $c_0$  is equal to 0.15;
- the gas is assumed to be ejected perpendicularly to the Roche surface with velocity  $u_0 = 0.0125$ .

The numerical boundary conditions are built using the standard procedure of solving of Riemann problem between two regions – one on the surface of the star and other corresponding to the nearest computational cell (see, e.g., [2, 12]).

The radius of the compact star is assumed to be equal to  $0.01A$ . Free outflow conditions are imposed on the accretor and on the outer boundary.

To solve the equations we use the TVD Roe scheme [22] of first order of approximation with monotonic flux limiters in form of Osher [23] that makes the scheme of third order of approximation. We also include Einfeldt modification of Roe scheme [24] to make the scheme more stable.

The computation domain for 2D case is a circle  $r \leq 3A$  (except the Roche lobe filled by mass-losing star and a circle representing the accretor) covered by the non-uniform grid containing  $231 \times 240$  gridpoints in  $r$  and  $\phi$  directions respectively. For 3D case the computation domain is a parallelepipedon  $[-A..2A] \times [-A..A] \times [0..A]$  (with the same exceptions) covered by the non-uniform grid containing  $132 \times 107 \times 30$  gridpoints in  $X$ ,  $Y$  and  $Z$  directions respectively. In both 2D and 3D the grids are condensed in the vicinity of accretor. In 3D runs symmetry about the equatorial plane is assumed. The numerical simulations are conducted up to nearly 10 orbital periods both for 2D and 3D cases.

## 2 COMPARISON OF 2D AND 3D RUNS

To perform the systematic comparison of the 2D and 3D models we conduct gasdynamical simulations for the same semidetached binary. The boundary conditions (density, gas velocity, and sound speed) at the surface of mass-losing star are kept constant in different runs, while the ratio  $\gamma$  of specific heats is a parameter to be varied. Four cases – two runs for  $\gamma = 1.01$  and  $\gamma = 1.2$  both in 2D and 3D models – are conducted. To study the influence of the numerical viscosity on the solution we have also conducted 2D runs (both for  $\gamma = 1.01$  and  $\gamma = 1.2$  cases) with the same coarse grid as we used for 3D model. The coarse-grid and fine-grid 2D solutions show the same structure of the gaseous flows in the system except the additional viscous broadening of shocks, therefore below we will describe the fine-grid 2D results.

Before describing the results of comparison it should be noted that the 3D solutions are a steady-state ones. In all 3D runs there are no changes of the flow structure for the time exceeding  $\sim 1.5$  orbital periods. The analysis of average characteristics of the obtained solutions shows that all parameters of the flow are stable in all 3D runs. For 2D case the solutions do not reach the steady-state and even for large evolution time quasi periodic

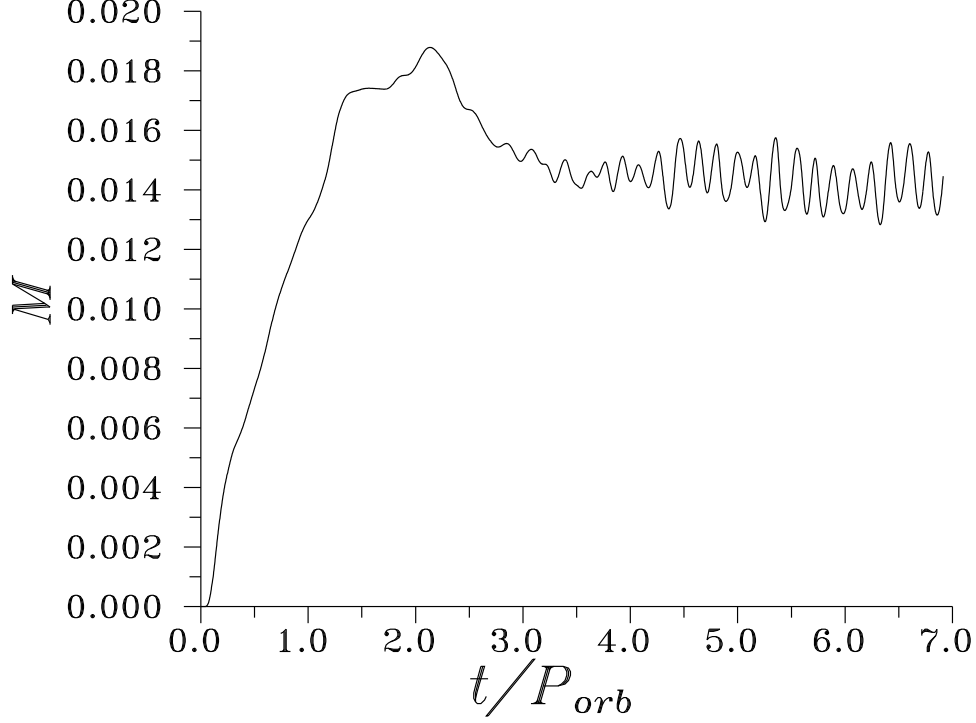


Figure 1: Surface mass ( $\int \rho dS$ ) contained in the circle with radius  $0.3A$  around accretor for 2D model with  $\gamma = 1.2$  as a function of time.

changes of the flow structure are observed. The confirmation of the non steady-state behavior of 2D solution can be got from the analysis of the average characteristics of the flow, e.g. from the consideration of the time-dependence of the mass variation in the fixed volume around accretor. In Figure 1 the surface mass ( $\int \rho dS$ ) contained in the circle with radius  $0.3A$  around accretor for  $\gamma = 1.2$  run is presented. It is seen that for the 2D solution the mass changes quasi periodically for all time. The observed oscillations are probably caused by restrictions of the 2D approach. The inconsistency of the mass accretion rate with the rate of mass transfer from the mass-losing star to accretion disk lead to non-steady-state behavior of the disk. Due to the absence of the  $Z$  motion of the gas in the 2D models the accumulated matter of the disk can exceed the limitation imposed by the gasdynamical structure of the flow. Then the excess of the matter tries to leave the system and as a consequence changes the gaseous flow structure. To compare the 2D and 3D models we extract the most typical characteristic features of the 2D flow patterns.

## 2.1 The case of $\gamma=1.01$

The general structure of gaseous flows in the equatorial plane of considered binary system for  $\gamma = 1.01$  case is presented in Figures 2–5. In Figures 2 and 3 the isolines of pressure and velocity vectors in the region  $[0..2A] \times [-0.8A..0.8A]$  are shown for 2D and 3D cases, respectively. The isolines of density, velocity vectors, and flowlines for the same runs in the region  $[0..1.5A] \times [-0.6A..0.6A]$  are presented in Figures 4 and 5. Figures are presented in

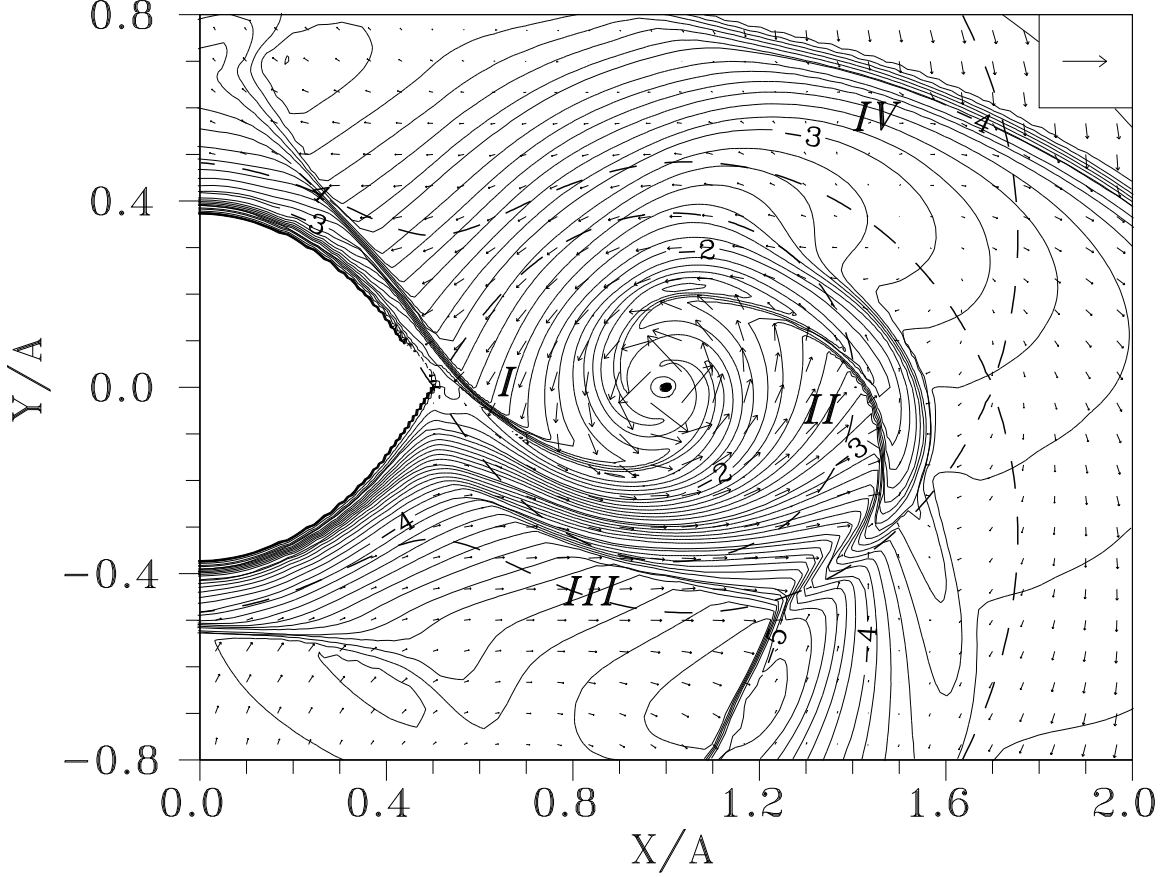


Figure 2: Pressure isolines and velocity vectors in the equatorial plane of the system for the 2D run (case  $\gamma = 1.01$ ) between  $10^{-5}$ ..0.2 with constant increment of  $\lg P$ . Digits on isolines denote values of  $\lg P$ . Roche equipotentials are shown by dashed lines. Shocks are marked by roman digits *I*, *II*, *III*, *IV*. The accretor is marked by the filled circle. Vector in the upper right corner corresponds to the value of velocity of  $3A\Omega$ .

rotating systems of coordinates with counter-clockwise directions of rotation and angular velocity  $\Omega$ . For 3D case arrows show the 3D velocities projected onto the slice plane.

The analysis of the results presented in Figures 2 and 3 shows that for considered near-isothermal case the flow structure obtained in 2D and 3D models have a set of common features: i) the accretion disk is formed; ii) there is a circumbinary envelope in the system; iii) the spiral-shaped shocks labeled by markers *I* and *II* are formed; iv) the interaction of the gas of the circumbinary envelope with the stream causes the formation of the shock wave labeled by marker *III*.

To make a more detailed analysis of the structures of gaseous flows let us consider the density fields and velocity vectors in the equatorial plane presented in Figures 4 and 5. In each figure three flowlines, labeled by markers "a", "b" and "c", are shown as well. These flowlines illustrate directions of matter flow in the system. The analysis of results presented in Figures 4 and 5 shows that for near-isothermal case the flow structure has the same characteristic features as it was discussed in our previous works [17, 18, 20]. The matter

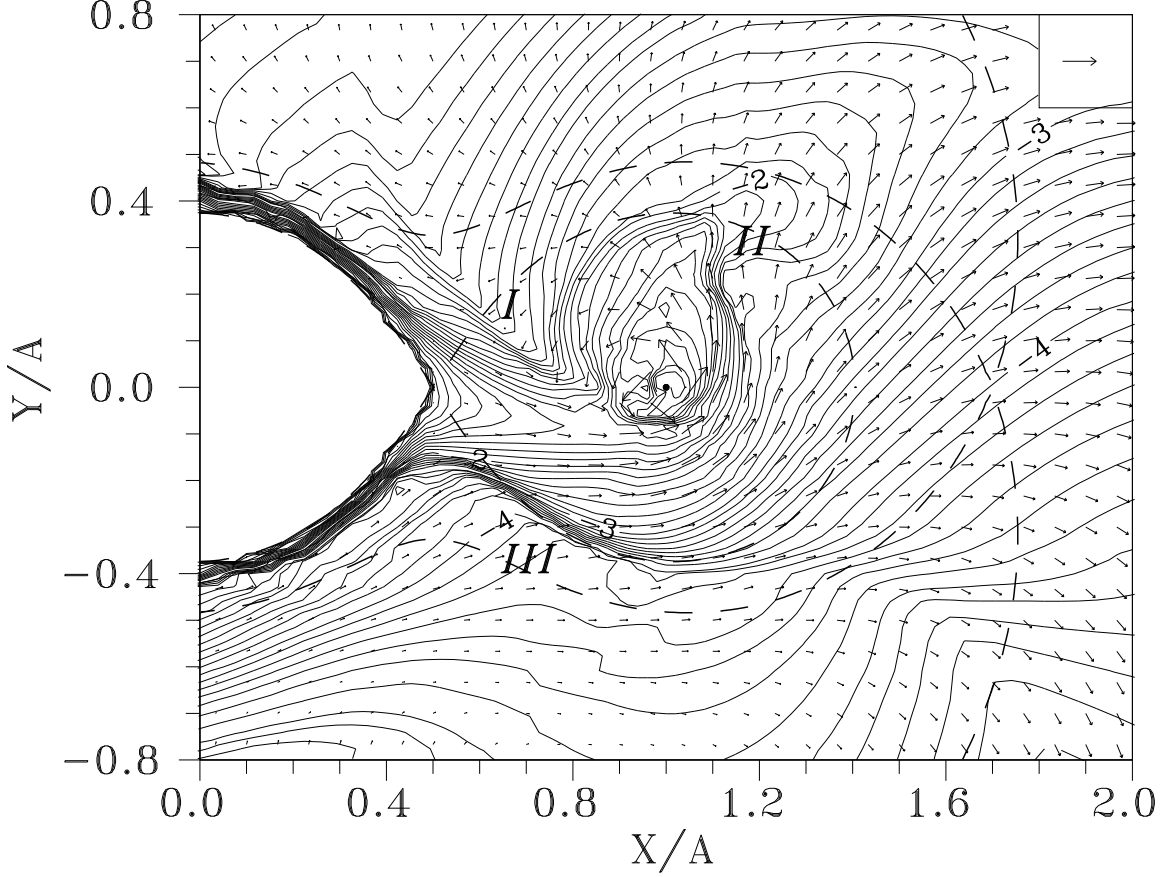


Figure 3: Pressure isolines and velocity vectors in the equatorial plane of the system for the 3D run (case  $\gamma = 1.01$ ) between  $10^{-5}$ ..0.2 with constant increment of  $\lg P$ . Digits on isolines denote values of  $\lg P$ . Roche equipotentials are shown by dashed lines. Shocks are marked by roman digits *I*, *II*, *III*. The accretor is marked by the filled circle. Vector in the upper right corner corresponds to the value of velocity of  $3A\Omega$ .

of the stream is redistributed into two parts: i) the first part (flowline "a") forms a quasi-elliptic accretion disk; ii) the second part (gas flows labeled by markers "b" and "c") forms the circumbinary envelope of the system. As it is seen from the figures the part of the circumbinary envelope makes a full revolution around the accretor (flowline "b") and mixes with the matter of the stream. This matter does not belong to the disk, because after mixing with the stream this gas can be considered as the stream itself. Part of the stream which does not interact with the disk immediately (flowlines "c" in Figs 4, 5) forms the outer part of the circumbinary envelope.

The presented flow structure shows that in our self-consistent solution the accretion disk is the part of the stream matter gravitationally captured by accretor. It is evident that the gas flow of the stream (deflected under the action of the gas of the circumbinary envelope) approaches the disk along the tangent line and does not cause the formation of the traditional "hot spot". On the other hand, the interaction between the gas of circumbinary envelope and the stream results in formation of an intensive shock wave *I*, located along the stream

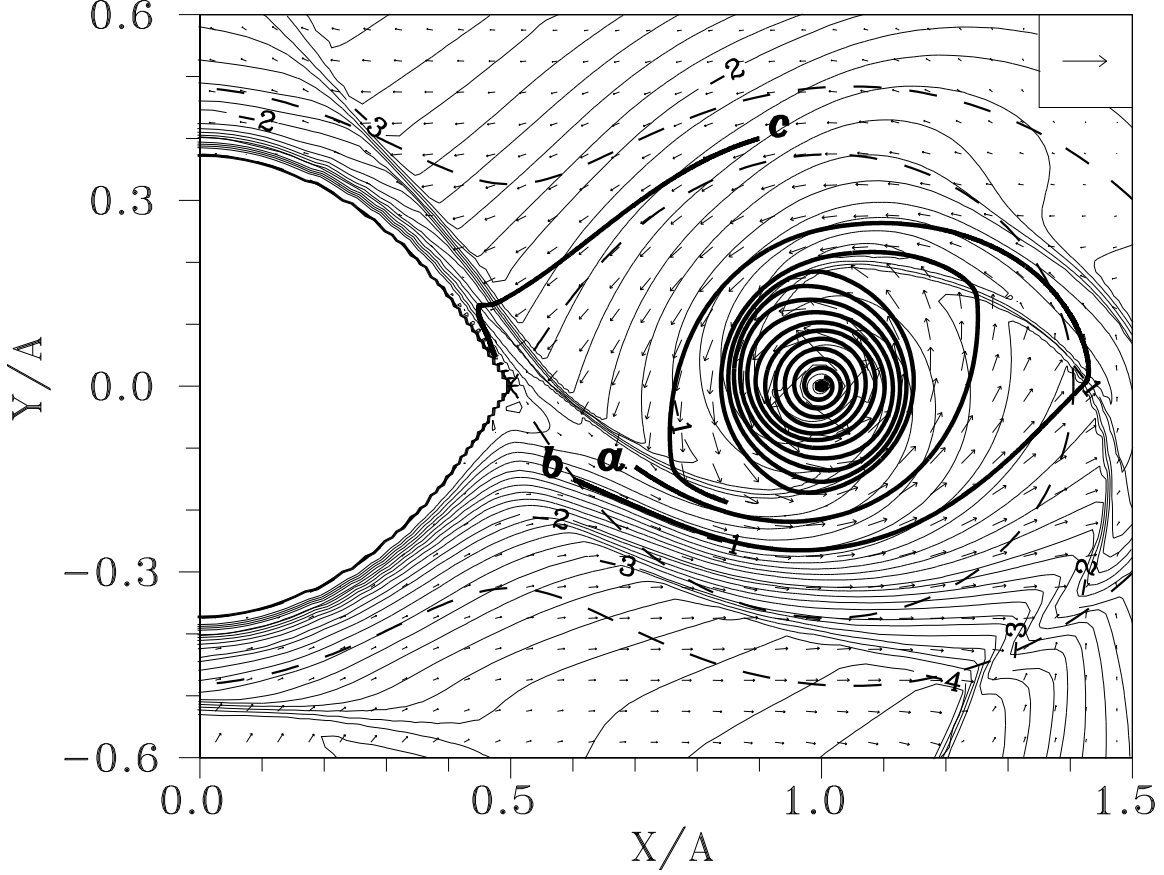


Figure 4: Density isolines and velocity vectors in the equatorial plane of the system for the 2D run (case  $\gamma = 1.01$ ) between  $10^{-5}$ ..5 with constant increment of  $\lg \rho$ . Digits on isolines denote values of  $\lg \rho$ . Different flowlines are marked by letters "a", "b", "c". Vector in the upper right corner corresponds to the value of velocity of  $3A\Omega$ .

edge turned towards orbital movement. As it is seen from the figures this shock arises not only at the stream edge, but also along the surface of Roche lobe, where the circumbinary envelopes interact with the mass-losing star. The interaction of the circumbinary envelope with the stream also leads to formation of rather intensive shock *III* at the other side of the stream, and of weak shock *II*, located at the boundary between the stream deviated by accretor and the gas of circumbinary envelope.

All characteristic feature for considered near-isothermal state are present both in 2D and 3D models. Nevertheless, as it follows from a comparison of the results presented in Figures 2–5 there are also some quantitative differences in the flow structures. In particular, in 3D case the accretion disk is rather small and the stream of the matter leaving  $L_1$  goes close to the accretor, while in 2D case the disk is large and more circular and the stream goes far from the accretor. This fact leads to redistribution of the gas fluxes in the system and, as a consequence, to small changes of the positions of the shocks *I*, *II*, *III*. Moreover, in 2D simulation we can see that the orbital motion of the accretor in the gas of the outer part of circumbinary envelope cause the formation in the system of the typical bow-shock



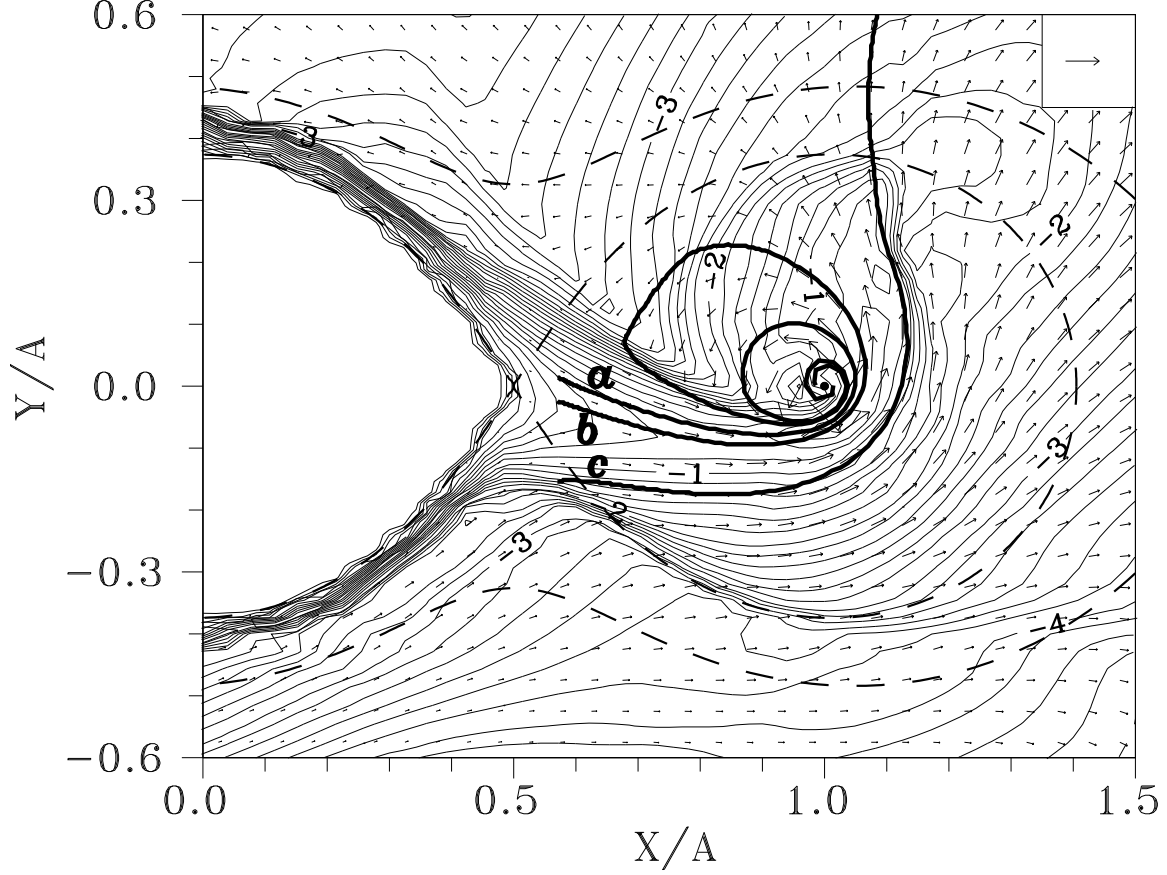


Figure 5: Density isolines and velocity vectors in the equatorial plane of the system for the 3D run (case  $\gamma = 1.01$ ) between  $10^{-5}$ ..1 with constant increment of  $\lg \rho$ . Digits on isolines denote values of  $\lg \rho$ . Different flowlines are marked by letters "a", "b", "c". Vector in the upper right corner corresponds to the value of velocity of  $3A\Omega$ .

labeled by  $IV$ , while in 3D case this bow shock does not arise. It is also seen that in 3D simulation the shock intensities are smaller than in 2D model (e.g. the intensity of shock  $II$  is so small that we can see it only in simulations using the scheme of the third order of approximation, while in the run of first order of approximation this shock disappear). The reasons of less intensities of the 3D shocks are rather evident and are due to the possibility of the gas motion in the  $Z$ -direction.

From the above description we may conclude that in spite of some quantitative differences in the results of 2D and 3D simulations the qualitative characteristics of the flow structures are similar. In turn, it means that the 2D models give a rather correct qualitative description of the gas flow structure for near-isothermal case.

## 2.2 The case of $\gamma=1.2$

In Figures 6–9 the results of 2D and 3D simulations are presented for the case  $\gamma=1.2$ . As in Figures 2, 3 the isolines of pressure and velocity vectors are shown in the same region of

equatorial plane for 2D (Fig. 6) and 3D (Fig. 7) cases. In Figures 8, 9 the isolines of density, velocity vectors, and flowlines are also presented.

Analysis of 2D results conducted for  $\gamma = 1.2$  (Figs 6, 8) allows to reveal the characteristic features of the flow structure. As it is seen from the Figures 6 and 8 the part of the stream (flowline "a" in Fig. 8) forms the accretion disk in the system. The higher value of adopted  $\gamma$  leads to less effective cooling of the disk (in comparison with  $\gamma = 1.01$  case), and, as a consequence, to formation of rather large disk. The stream-disk interaction is shock free. As in the  $\gamma = 1.01$  case the forming circumbinary envelopes (flowlines "b", "c" in Fig. 8) interacts with stream and the surface of mass-losing star and leads to formation of the shocks *I–III*. The bow shock *IV* caused by orbital motion of the accretor in the circumbinary envelope is also present in the calculated flow structure. The most important changes are related with the positions of spiral-shaped shocks *I*, and *II*. For considered case of  $\gamma = 1.2$  the shocks *I* and *II* go through the disk up to accretor. Assuming that these shocks are caused by the interaction of the circumbinary envelope with the stream (as in the case of  $\gamma = 1.01$ ) their behavior is somehow predictable. For shock formed due to colliding of flow with obstacle the distance between obstacle and shock increases with increasing of  $\gamma$  [25]. So the shock *I* has to form at some distance from the stream, while for  $\gamma = 1.01$  it is placed on the edge of the stream. If the shock is in the disk it has to propagate to the inner part due to circular motion of the gas around accretor. In considered case the shocks are strong enough and stopped directly at the accretor surface. The same explanation can be applied for describing the changing of the shock *II* position for  $\gamma = 1.2$  case.

From the above comparison of 2D runs conducted at different  $\gamma$  it is seen that for 2D case the solution does not change drastically. All characteristic features of the flow structure (accretion disk, gas fluxes, shocks *I–IV*) are the same, and there are only quantitative changes. It should be also noted that the described 2D flow structures are close to that obtained in 2D simulations of Sawada et al. [2, 3]. The observed quantitative changes are not very significant and can be explained by changing of adopted value of  $\gamma$ .

The dependence of the 3D solution from the chosen value of  $\gamma$  is more significant than in 2D case. Comparison of 3D flow structures obtained at  $\gamma=1.01$  (Figs 3, 5) and at  $\gamma=1.2$  (Figs 7, 9) shows the drastic changes in the flow pattern. The details of these changes will be described in the next section. Here we simply indicate that for more high value of  $\gamma$  the 3D solution (Figs 7, 9) is different from the 2D one (Figs 6, 8). In particular, in 3D case the matter of the stream does not form the accretion disk. Moreover, due to redistributing of the gas fluxes in the system the only one spiral-shaped shock *I* is formed in the system, while the shock *II* is disappeared.

Resuming the above points, we may conclude that for near-isothermal case the 2D and 3D solutions are qualitative similar. For more high  $\gamma$  obtained in 2D and 3D models solutions are different. This difference is caused by changing of the 3D flow patterns obtained at different  $\gamma$ , while the 2D solutions are comparable and keep all characteristic features for both considered cases ( $\gamma = 1.01$  and  $\gamma = 1.2$ ). This conclusion is in a good agreement with study carried out by Fridman & Khoruzhii [21] where they have analytically shown that for non-self-gravitational accretion disk the 2D approach gives an adequate solution only for isothermal case, while for all other cases the only 3D models are valid.

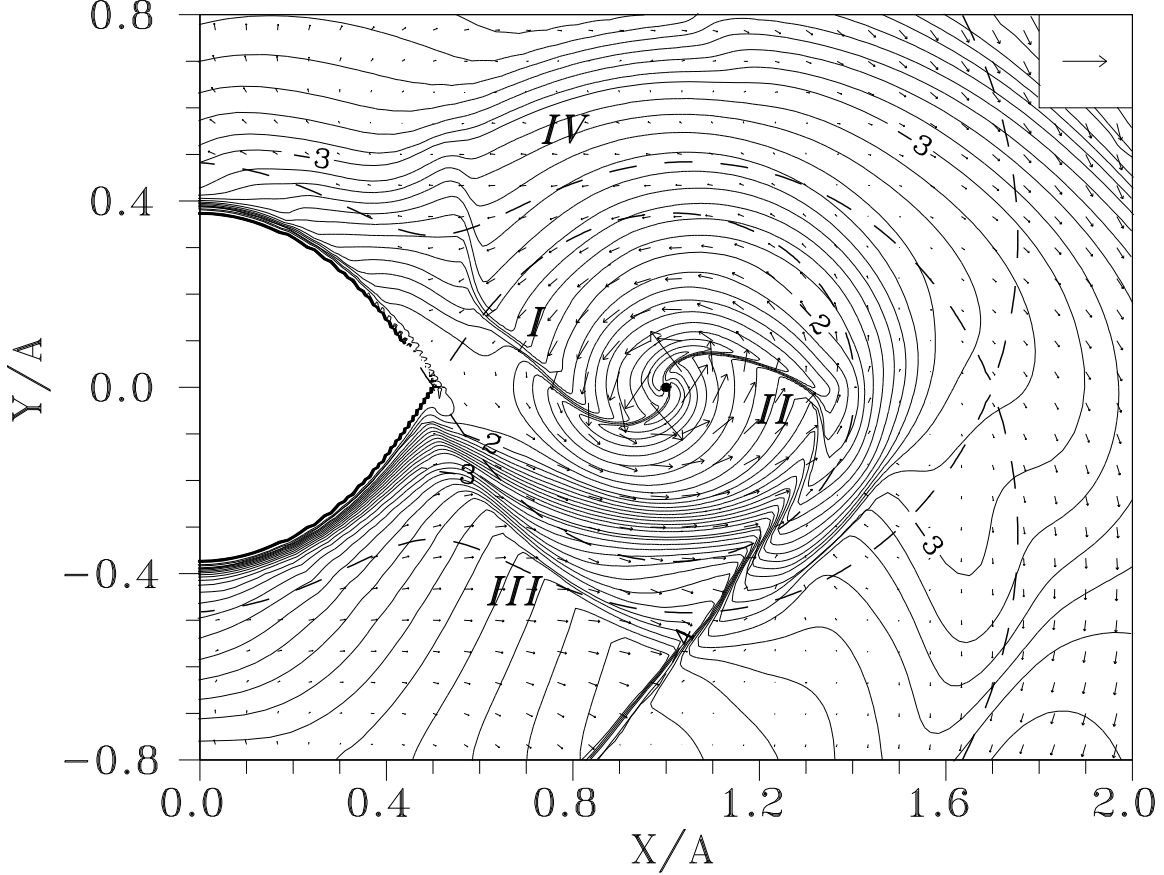


Figure 6: Pressure isolines and velocity vectors in the equatorial plane of the system for the 2D run (case  $\gamma = 1.2$ ) between  $10^{-5}$ ..0.2 with constant increment of  $\lg P$ . Digits on isolines denote values of  $\lg P$ . Roche equipotentials are shown by dashed lines. Shocks are marked by roman digits *I*, *II*, *III*, *IV*. The accretor is marked by the filled circle. Vector in the upper right corner corresponds to the value of velocity of  $3A\Omega$ .

### 3 3D FLOW STRUCTURE AT DIFFERENT $\gamma$

As it follows from the comparison of the 3D results obtained for  $\gamma = 1.01$  (Figs 3, 5) and  $\gamma = 1.2$  (Figs 7, 9) the flow structures in these cases are strongly different. The main difference is the absence of the accretion disk for the case of higher  $\gamma$ .

For more high value of  $\gamma$  (Figs 7, 9) the stream goes very close to accretor. This leads to the direct interaction of the stream with accretor (flowline "a") without forming of the accretion disk. As a consequence, in steady-state regime for run with  $\gamma = 1.2$  the fraction of accreted matter is approximately equal to 39% of the total amount of matter injected into the system by the donor star, while for near-isothermal case this value is equal to 68%. Redistribution of the gas fluxes in the system results in changing of the positions and intensities of shocks *I* and *III*, and disappearing of shock *II*.

As it is seen from the analysis of results the 3D solutions obtained at different  $\gamma$  are qualitative different, while 2D solutions have the same features of the gas flow structure.

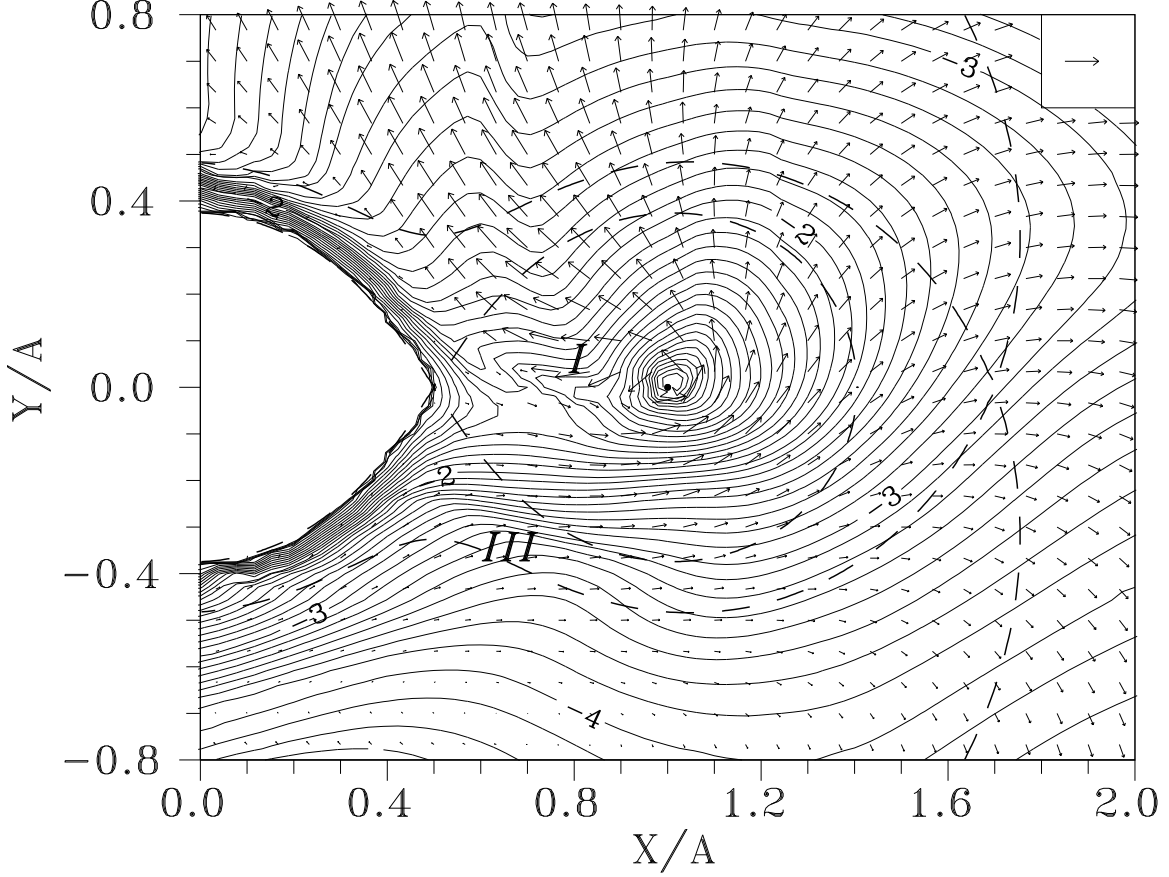


Figure 7: Pressure isolines and velocity vectors in the equatorial plane of the system for the 3D run (case  $\gamma = 1.2$ ) between  $10^{-5}$ ..0.2 with constant increment of  $\lg P$ . Digits on isolines denote values of  $\lg P$ . Roche equipotentials are shown by dashed lines. Shocks are marked by roman digits *I* and *III*. The accretor is marked by the filled circle. Vector in the upper right corner corresponds to the value of velocity of  $3A\Omega$ .

Probably this is connected with the changing of the 3D flow patterns in the third ( $Z$ ) direction. In Figures 10 and 11 density isolines from  $\rho \sim 0.1$  up to the value 0.001 and velocity vectors are shown for cases  $\gamma = 1.01$  and  $\gamma = 1.2$ , respectively. These results are presented in the  $YZ$  plane, passing through the accretor and which is perpendicular to the line connecting the centers of stars. From these results it is seen that for near-isothermal case (Fig. 10) the well defined accretion disk is formed. It is also seen that in this case the matter moves from the higher altitudes to the accretor. For case of  $\gamma = 1.2$  (Fig. 11) the disk is not formed and the direction of the gas motion is different - the matter moves to the high altitudes. With the increasing of specific heats ratio  $\gamma$  the compressibility of the gas is decreased. On the other hand the higher value of  $\gamma$  mimics the case with less cooling efficiency. It means that pressure and temperature for the  $\gamma = 1.2$  case are higher than in the near-isothermal case. In turn, these facts lead to the solution without accretion disk and gas outflow from the equatorial plane.

Obtained results are in a good agreement with the 3D simulations made by Molteni et

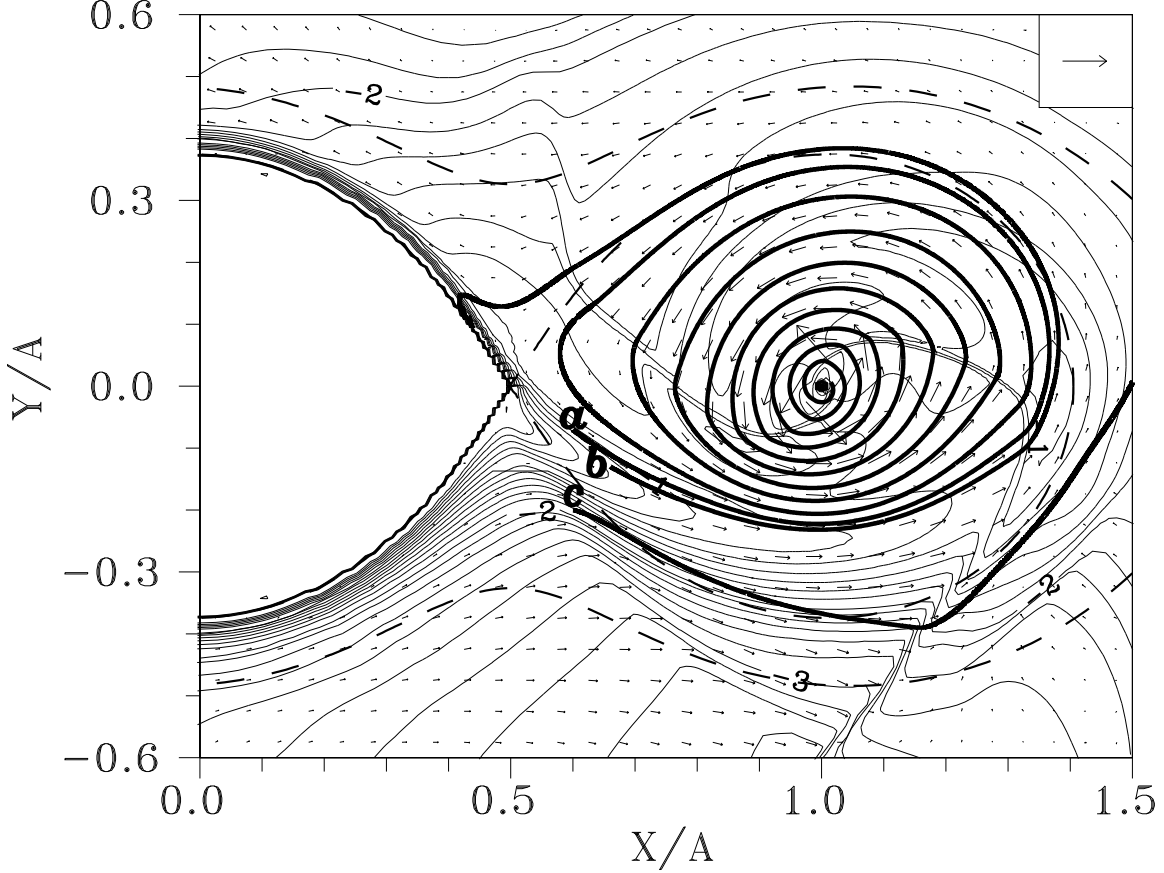


Figure 8: Density isolines and velocity vectors in the equatorial plane of the system for the 2D run (case  $\gamma = 1.2$ ) between  $10^{-5}$ ..5 with constant increment of  $\lg \rho$ . Digits on isolines denote values of  $\lg \rho$ . Different flowlines are marked by letters "a", "b", "c". Vector in the upper right corner corresponds to the value of velocity of  $3A\Omega$ .

al. [11] and by Lanzafame et al. [13], where it was found that the accretion disk does not exist for  $\gamma \geq 1.1$ . The comparison of the results of different authors shows that the critical value of  $\gamma$  at which the disk does not form depends on the used numerical scheme and model parameters.

## 4 WHAT ARE THE REASONS OF THE SPIRAL-SHAPED SHOCKS FORMATION?

The results presented above show the formation of the spiral-shaped shocks *I* and *II* in the considered binary. The obtained flow structures are close to ones described in works [2, 3] for 2D models and in works [12, 19] for 3D model. In a set of previous works (see, e.g., [2–5, 12, 19]) these shocks were explained as an intrinsic spirals caused by tidal disturbances.

The numerical simulations conducted in this work result in suspicion that the obtained spiral-shaped shocks are due to colliding of the gas fluxes in the system. The more fine grid

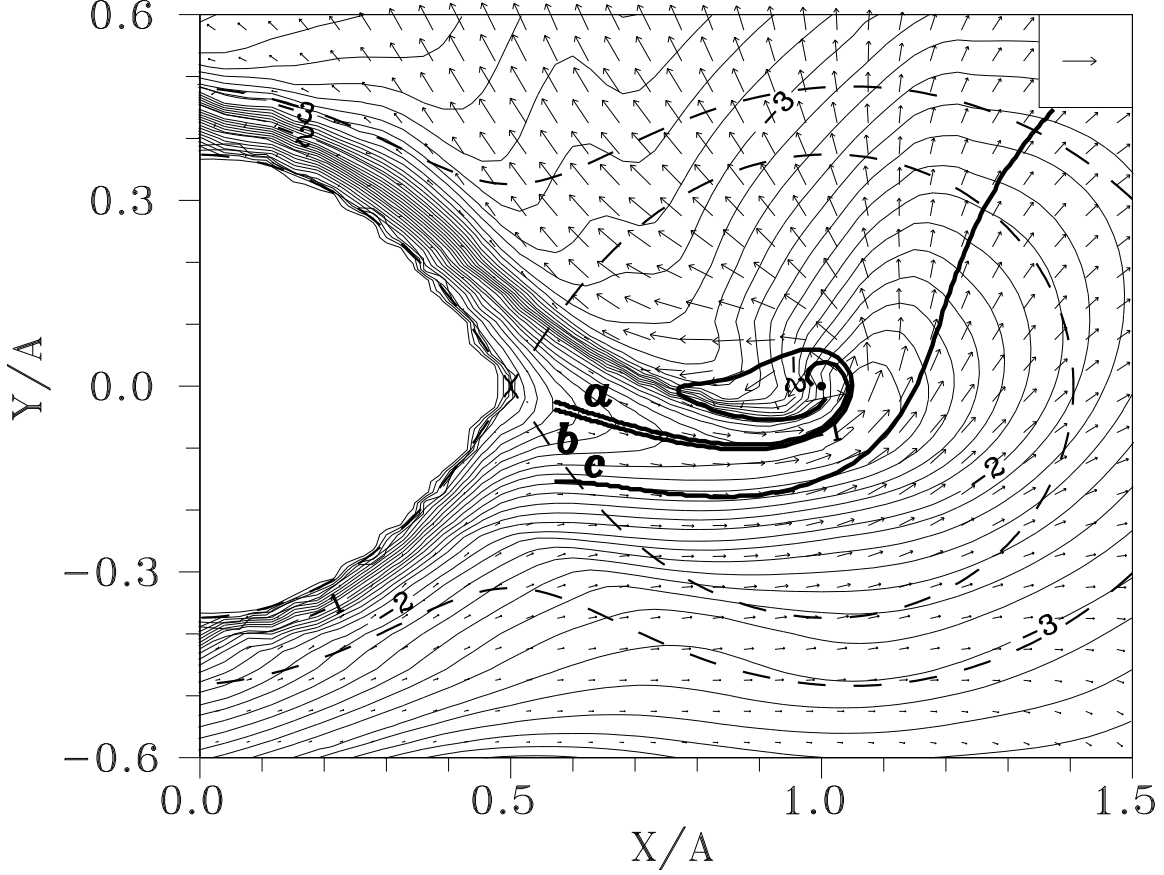


Figure 9: Density isolines and velocity vectors in the equatorial plane of the system for the 3D run (case  $\gamma = 1.2$ ) between  $10^{-5}$ ..1 with constant increment of  $\lg \rho$ . Digits on isolines denote values of  $\lg \rho$ . Different flowlines are marked by letters "a", "b", "c". Vector in the upper right corner corresponds to the value of velocity of  $3A\Omega$ .

used in our models permits us to consider the details of the flow structure and to emphasize the features proving the "flow crossing" nature of these shocks. The analysis of results shows, that the spiral-shaped shock *I* is caused by the striking of the gas of circumbinary envelope revolved around accretor with the edge of the stream. The second spiral-shaped shock *II* (in numerical models where it is present) is also caused by colliding of the stream with the gas of circumbinary envelope. The analysis of the gas flow motion presented in Figures 2–9 argues this point.

An additional argument on the "flow-crossing" nature of the shocks *I* and *II* can be obtained from the consideration of the shocks positions and their lengths. As it is seen from Figures 2–9 the spiral-shaped shocks are rather long and propagate far from the accretion disk. The ending points of the shocks are located in regions where the tidal disturbances are very small and can not generate the shocks. It is also seen from the Figures 2–9 the spiral-shaped shocks *I*, *II* (as well as non-spiral shocks *III*, *IV*) have the double-shock structures. This is typical for shocks arising between colliding flows and can be considered as an decisive prove of the "flow-crossing" nature of these shocks.

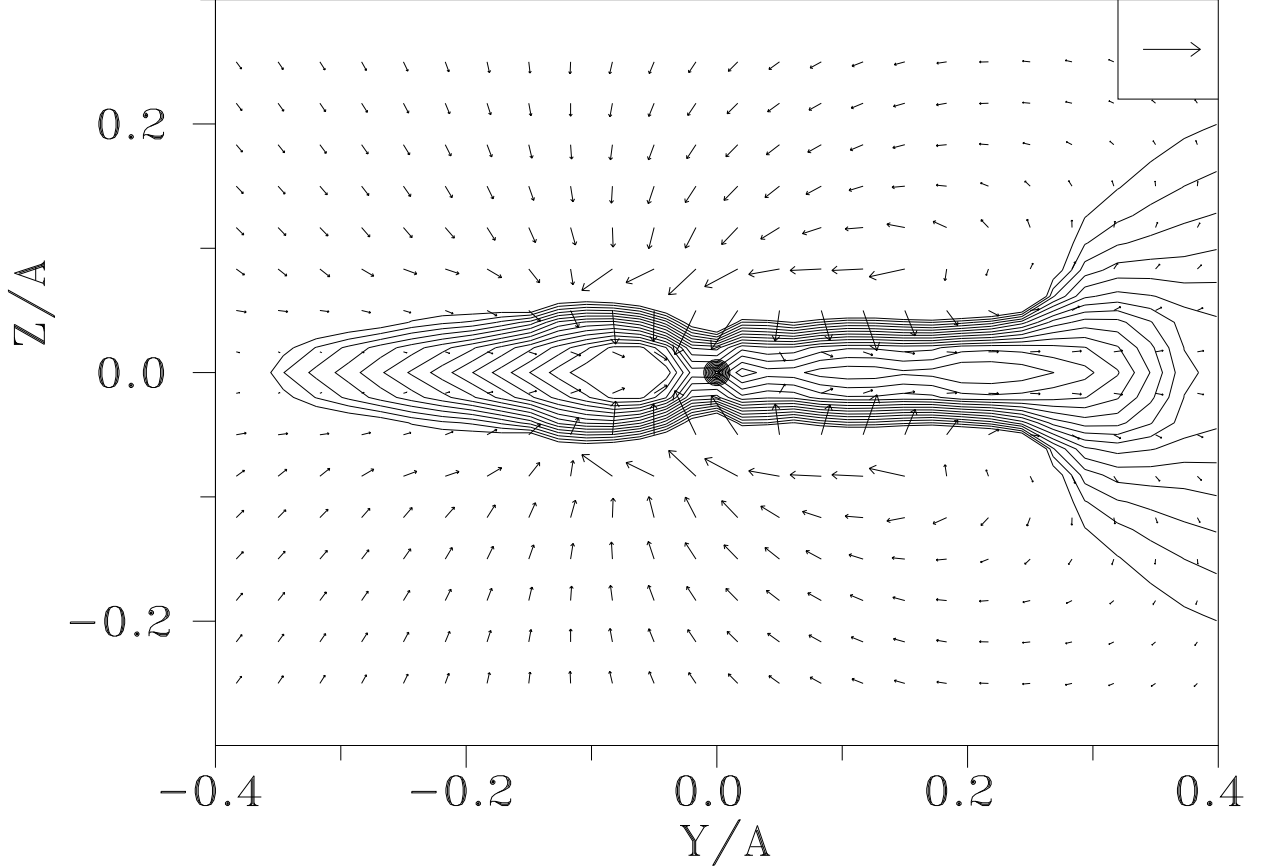


Figure 10: Density isolines and velocity vectors in  $YZ$  plane passing through accretor (case  $\gamma = 1.01$ ). Logarithmic contours are plotted, starting from density of 0.001..0.1 (maximum is reached in equatorial plane  $z = 0$ ). The accretor is marked by the filled circle. Vector in the upper right corner corresponds to the value of velocity of  $6A\Omega$ .

It should be noted that in our simulations we have not found the formation of the tidally induced intrinsic spiral shocks in the accretion disk. Probably this is related to the numerical restrictions (number of grid points, scheme viscosity, etc.) of the model we used, and it is possible to get a flow structure containing both "flow-crossing" and intrinsic spiral shocks, although there are some theoretical indications that at small  $\gamma$  ( $\gamma < 1.16$ ) the formation of spiral shocks is not possible [26]. From the other hand we can not assert that these shocks will not arise in simulations of binaries with different binary parameters.

## 5 CONCLUSIONS

The presented results of systematic comparison of 2D and 3D numerical models show that only for case of  $\gamma \sim 1$  the obtained solutions are qualitatively similar. For higher value of  $\gamma$  there are strong differences between flow structures obtained in 2D and 3D models. This means that the 2D models give a rather adequate results only for near-isothermal case. These conclusions are in a good agreement with analytical work [21].

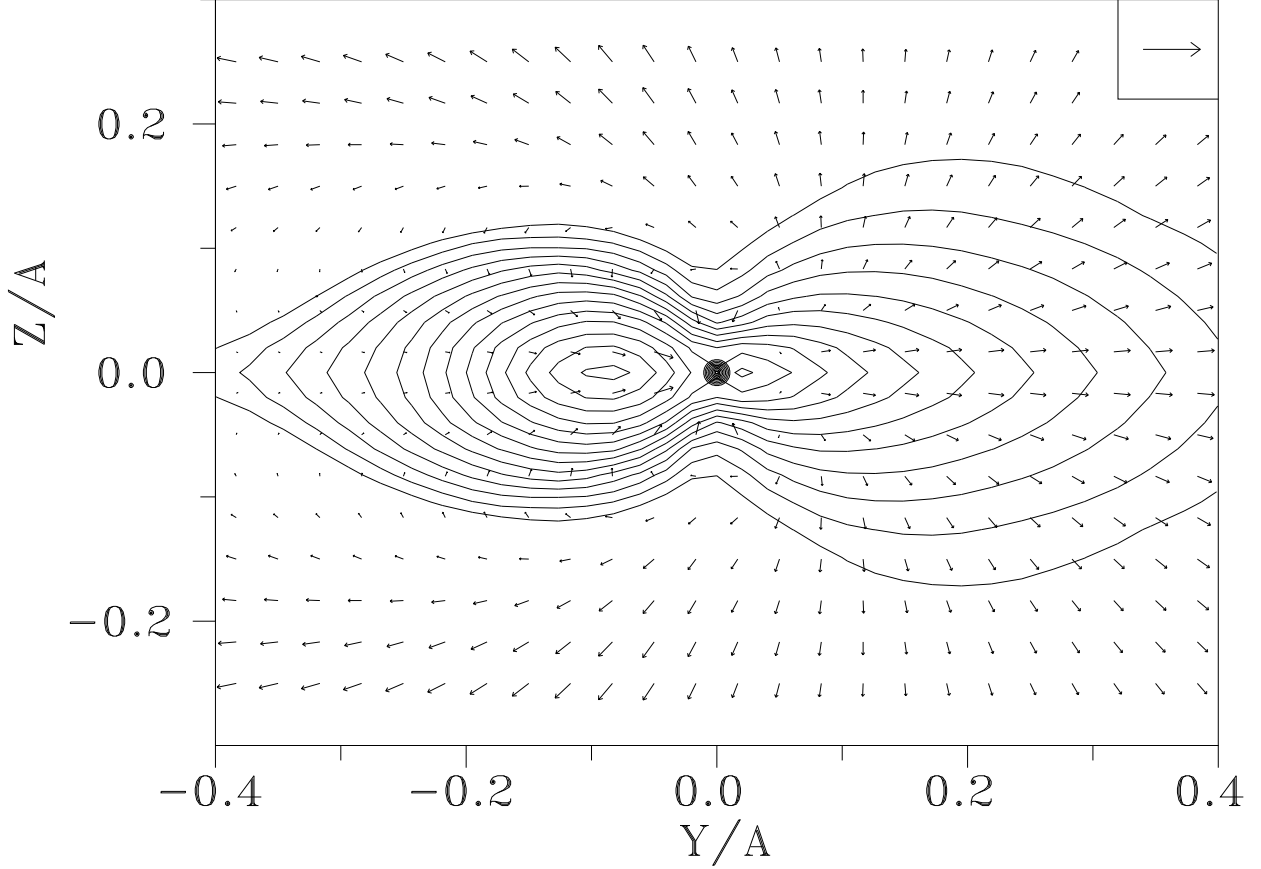


Figure 11: Density isolines and velocity vectors in  $YZ$  plane passing through accretor (case  $\gamma = 1.2$ ). Logarithmic contours are plotted between 0.001..0.1 (maximum is reached in equatorial plane  $z = 0$ ). The accretor is marked by the filled circle. Vector in the upper right corner corresponds to the value of velocity of  $6A\Omega$ .

The revealed differences between 2D and 3D models are due to the drastic changing of the 3D flow structure in dependence of adopted value of  $\gamma$ , while the 2D models give a qualitatively similar solutions at different  $\gamma$ . The main differences between 3D runs conducted for  $\gamma = 1.01$  and  $\gamma = 1.2$  are the absence of the accretion disk for higher value of  $\gamma$  and the redistribution of the gas flows in the system.

The spiral-shaped shock waves obtained in presented models are similar to shocks observed in other numerical simulations (see, e.g., [2, 3, 12, 19]). In contradiction to previous authors, who believe that these shocks are intrinsic spirals caused by tidal disturbances, we suggest the "flow-crossing" origin of these shocks. The analysis of the presented results proves this conclusion and shows that the spiral-shaped shocks are due to collisions of the gaseous flows in the system.



# ACKNOWLEDGMENTS

This work was supported by the Russian Foundation for Basic Research (grant 99-02-17619) and by grant of President of Russia (99-15-96022).

# REFERENCES

1. Prendergast, K.H., *Astrophys. J.*, 1960, vol.132, p.162.
2. Sawada, K., Matsuda, T., and Hachisu, I., *Mon. Not. R. Astron. Soc.*, 1986, vol.219, p.75.
3. Sawada, K., Matsuda, T., Inoue, M., and Hachisu, I., *Mon. Not. R. Astron. Soc.*, 1987, vol.224, p.307.
4. Spruit, H.C., *Astron. Astrophys.*, 1987, vol.184, p.173.
5. Różyczka, M., and Spruit, H.C., in *Theory of accretion disks*, ed. F.Meyer et al., Dordrecht: Kluwer, 1989, p.341.
6. Taam, R.E., Fu, A., and Fryxell, B.A., *Astrophys. J.*, 1991, vol.371, p.696.
7. Blondin, J.M., Richards, M.T., and Malinowski, M.L., *Astrophys. J.*, 1995, vol.445, p.939.
8. Murray, J.R., *Mon. Not. R. Astron. Soc.*, 1996, vol.279, p.402.
9. Nagasawa, M., Matsuda, T., and Kuwahara, K., *Numer. Astrophys. in Japan*, 1991, vol.2, p.27.
10. Hirose, M., Osaki, Y., and Minishige, S., *Publ. Astron. Soc. Japan*, 1991, vol.43, p.809.
11. Molteni, D., Belvedere, G., and Lanzafame, G., *Mon. Not. R. Astron. Soc.*, 1991, vol.249, p.748.
12. Sawada, K., and Matsuda, T., *Mon. Not. R. Astron. Soc.*, 1992, vol.255, p.17P.
13. Lanzafame, G., Belvedere, G., and Molteni, D., *Mon. Not. R. Astron. Soc.*, 1992, vol.258, p.152.
14. Belvedere, G., Lanzafame, G., and Molteni, D., *Astron. Astrophys.*, 1993, vol.280, p.525.
15. Meglicki, Z., Wickramasinghe, D., and Bicknell, G.V., *Mon. Not. R. Astron. Soc.*, 1993, vol.264, p.691.
16. Lanzafame, G., Belvedere, G., and Molteni, D., *Mon. Not. R. Astron. Soc.*, 1994, vol.267, p.312.
17. Bisikalo, D.V., Boyarchuk, A.A., Kuznetsov, O.A., and Chechetkin, V.M., *Astron. Zh.*, vol.74, p.880 (*Astron. Reports*, 1997, vol.41, p.786, preprint astro-ph/9802004).
18. Bisikalo, D.V., Boyarchuk, A.A., Kuznetsov, O.A., and Chechetkin, V.M., *Astron. Zh.*, vol.74, p.889 (*Astron. Reports*, 1997, vol.41, p.794, preprint astro-ph/9802039).

19. Yukawa, H., Boffin, H.M.J., and Matsuda, T., *Mon. Not. R. Astron. Soc.*, 1997, vol.292, p.321.
20. Bisikalo, D.V., Boyarchuk, A.A., Chechetkin, V.M., Kuznetsov, O.A., and Molteni, D., *Mon. Not. R. Astron. Soc.*, 1998, vol.300, p.39.
21. Fridman, A.M., and Khoruzhii, O.V., in Gor'kavyi, N.N., Fridman, A.M., *Physics of planetary rings*, Moscow: Nauka, 1994, p. 282 (in Russian).
22. Roe, P.L., *Ann. Rev. Fluid Mech.*, 1986, vol.18, p.337.
23. Chakravarthi, S., and Osher, S., *AIAA Pap.*, 1985, N 85-0363.
24. Einfeldt, B., *SIAM J. Numer. Anal.*, 1988, vol.25, p.294.
25. Landau, L.D., and Lifshitz, E.M., *Fluid mechanics*, Elmsford: Pergamon Press, 1959.
26. Chakrabarty, S.K., *Mon. Not. R. Astron. Soc.*, 1992, vol.259, p.410.